

Enhanced sampling of multidimensional free-energy landscapes using adaptive biasing forces

Christophe Chipot*and Tony Lelièvre†

**Theoretical and Computational Biophysics Group,
Beckman Institute for Advanced Science and Engineering,
University of Illinois, Urbana-Champaign.*

†Université Paris-Est, Cermics.

October 23, 2018

Abstract

We propose an adaptive biasing algorithm aimed at enhancing the sampling of multimodal measures by Langevin dynamics. The underlying idea consists in generalizing the standard adaptive biasing force method commonly used in conjunction with molecular dynamics to handle in a more effective fashion multidimensional reaction coordinates. The proposed approach is anticipated to be particularly useful for reaction coordinates, the components of which are weakly coupled, as illuminated in a mathematical analysis of the long-time convergence of the algorithm. The strength as well as the intrinsic limitation of the method are discussed and illustrated in two realistic test cases.

1 Introduction

Sampling of multimodal measures is a central problem in many scientific areas, such as statistical simulations, in particular molecular dynamics, which constitutes the primary focus of the present work. One standard approach to deal with such a situation consists in resorting to biasing techniques — e.g. importance sampling methods, in order to reduce the multimodal nature of the targeted measure. Under these premises, the main difficulty is evidently to devise the correct bias.

One class of methods proposed in the framework of molecular dynamics and which has proven to be useful also for a variety of applications [15] are adaptive biasing numerical schemes. The underlying idea here consists in designing adaptively the bias such that the new targeted measure be uniform along *a priori* chosen directions. Only these directions have to be chosen, but not the precise analytical expression of the bias. Examples of such class of approaches include the Wang-Landau algorithm [58], non-equilibrium metadynamics [33, 11] and the adaptive biasing force (ABF) method [17, 26], which will constitute the main thrust of this contribution. The reader is referred to [39, Chapter 5] for a general, mathematically-oriented presentation of adaptive methods.

Let us introduce the ABF method. In what follows, the algorithms will be presented in the framework of sampling of configurational space and overdamped Langevin

*On leave from Équipe de dynamique des assemblages membranaires, UMR 7565, Nancy Université, BP 239, 54506 Vandœuvre-lès-Nancy cedex, France. chipot@ks.uiuc.edu

†École des Ponts ParisTech, 6 et 8 avenue Blaise Pascal, 77455 Marne-la-Vallée, France. lelievre@cermics.enpc.fr

dynamics, but generalization to sampling of phase space and standard Langevin dynamics is straightforward, as can be seen in Section 4. The canonical, Boltzmann-Gibbs, measure will be considered here:

$$d\mu(q) = Z^{-1} \exp(-\beta V(q)) dq, \quad (1)$$

where β is proportional to the inverse temperature, $q \in \mathcal{D}$, $V : \mathcal{D} \rightarrow \mathbb{R}$ is the so-called potential energy function, which is assumed to be a smooth function in the following, $Z = \int_{\mathcal{D}} \exp(-\beta V(q)) dq$ and $\mathcal{D} = \{q, V(q) < \infty\}$ is the configurational space. The overdamped Langevin dynamics writes:

$$dQ_t = -\nabla V(Q_t) dt + \sqrt{2\beta^{-1}} dB_t, \quad (2)$$

where B_t is an n -dimensional standard Brownian motion. Under mild conditions on V , this dynamics is ergodic with respect to the measure μ , i.e. trajectory or time averages converge to canonical averages.

For a multimodal measure μ , the sampling obtained with Q_t is, however, rather poor. Indeed, the typical problem with dynamics (2) is that the process Q_t remains trapped for long times in some metastable states. The purpose of an adaptive biasing force is to enhance sampling by subtracting from V a potential such that the aforementioned metastable features are eliminated. This relies on an assumed *a priori* knowledge of those “coordinates” that remain trapped — viz. “slow variables” of the dynamics, also called “collective variables” or “reaction coordinates”. This method can thus be seen as an adaptive importance sampling method.

In the following, emphasis will be put on the case where two slow variables have been identified, namely $\xi_1 : \mathcal{D} \rightarrow \mathbb{T}$, and $\xi_2 : \mathcal{D} \rightarrow \mathbb{T}$, where \mathbb{T} denotes the one-dimensional torus. Throughout the present work, ξ_1 and ξ_2 will be assumed to be smooth functions such that $|\nabla \xi_1| \neq 0$ and $|\nabla \xi_2| \neq 0$.

For simplicity, let us consider for the moment simple reaction coordinates:

$$\mathcal{D} = \mathbb{T}^n, \xi_1(x) = x_1, \xi_2(x) = x_2, \quad (3)$$

where the components of x are referred to as: $x = (x_1, x_2, x_{3\dots n})$. The case of general ξ_i 's will be discussed below, in Sections 3 and 4. In this simple framework, one standard ABF-like method is [37]:

$$\begin{cases} dY_t = \left(-\nabla V + \sum_{\alpha=1}^2 \Gamma_t^\alpha \circ (\xi_1, \xi_2) \nabla \xi_\alpha \right) (Y_t) dt + \sqrt{2\beta^{-1}} dB_t, \\ \text{for } \alpha = 1, 2, \Gamma_t^\alpha(x_1, x_2) = \mathbb{E}(\partial_{x_\alpha} V(Y_t) | (\xi_1, \xi_2)(Y_t) = (x_1, x_2)). \end{cases} \quad (4)$$

In practice, the dynamics is discretized in time, and the biasing forces, Γ_t^α , are approximated by empirical or time averages in each cells of a grid of the values of (ξ_1, ξ_2) . The bottom line of the method is to observe that, in the long-time limit, (Γ_t^1, Γ_t^2) converges to ∇A , where A is the so-called free energy associated to V and (ξ_1, ξ_2) — see [38]. At equilibrium, the potential eventually becomes $V - A \circ (\xi_1, \xi_2)$, which is such that the associated Boltzmann-Gibbs measure, proportional to $\exp(-\beta(V - A \circ (\xi_1, \xi_2)))$, has uniform marginal laws along (ξ_1, ξ_2) . Indeed, the free energy is defined, up to an additive constant, as:

$$A(x_1, x_2) = -\beta^{-1} \ln \left(\int \exp(-\beta V(x_1, x_2, x_{3\dots n})) dx_{3\dots n} \right). \quad (5)$$

Using the definition (5) of the free energy A , it is easy to check that the equilibrium probability density for (4), namely

$$\psi_\infty(x_1, x_2, x_{3\dots n}) \propto \exp \left(-\beta(V(x_1, x_2, x_{3\dots n}) - A(x_1, x_2)) \right)$$

is such that the marginal law of ψ_∞ along (ξ_1, ξ_2) is uniform:

$$\int_{\mathbb{T}^{n-2}} \psi_\infty(x_1, x_2, x_{3\dots n}) dx_{3\dots n} = 1_{\mathbb{T}^2}.$$

Another related important property of the stochastic differential equation (4) is that the dynamics along (ξ_1, ξ_2) has a simple diffusive behavior, since, by a straightforward Itô calculus, for any test function $\varphi : \mathbb{T}^2 \rightarrow \mathbb{R}$,

$$\partial_t \mathbb{E}(\varphi((\xi_1, \xi_2)Y_t)) = \beta^{-1} \mathbb{E}(\Delta\varphi((\xi_1, \xi_2)Y_t)) \quad (6)$$

which is a weak form for the heat equation on the marginal law along (ξ_1, ξ_2) of the density of Y_t . Roughly speaking, the energy landscape has been flattened in the (ξ_1, ξ_2) -direction.

The aim of this work is to explore a generalization of the ABF method — originally devised to compute a free-energy difference, which is a quantity of paramount importance in statistical mechanics [14, 39] — focusing primarily on its adaptive importance sampling feature and with the objective of obtaining a diffusion along some chosen directions. More specifically, we have in mind the case of m reaction coordinates with $m \geq 4$, for which the standard ABF approach cannot be used, because it would require that the biasing forces, namely m functions of m variables, be approximated by a Monte Carlo procedure which is admittedly computationally prohibitive as m increases. Moreover, the fact that the biased dynamics along the reaction coordinates is a simple diffusion in the whole torus \mathbb{T}^m seems somewhat inappropriate, given that exploration of such a space may become extraordinarily long for large m .

The approach proposed herein consists in considering the dynamics:

$$\begin{cases} dX_t = -\nabla \left(V - \sum_{\alpha=1}^2 A_t^\alpha \circ \xi_\alpha \right) (X_t) dt + \sqrt{2\beta^{-1}} dB_t, \\ \text{for } \alpha = 1, 2, \frac{dA_t^\alpha}{dx_\alpha}(x_\alpha) = \mathbb{E}(\partial_{x_\alpha} V(X_t) | \xi_\alpha(X_t) = x_\alpha). \end{cases} \quad (7)$$

The interest of this dynamics is that only two one-dimensional functions have to be approximated. It is, therefore, expected that the Monte Carlo approximation of the biasing functions will be faster. One can check that this dynamics retains some essential features of the ABF dynamics (4), namely the fact that it leads to a simple diffusive behavior *in each direction* ξ_α (see Section 2.1 below): for any test function $\varphi : \mathbb{T} \rightarrow \mathbb{R}$, and for $\alpha \in \{1, 2\}$,

$$\partial_t \mathbb{E}(\varphi(\xi_\alpha(X_t))) = \beta^{-1} \mathbb{E}(\varphi''(\xi_\alpha(X_t))).$$

As a consequence, the marginal laws along ξ_1 and along ξ_2 of the equilibrium measure of the dynamics are uniform laws over \mathbb{T} . It ought to be noted, however, that (6) does not hold in general in such a situation, and that the marginal law of the equilibrium measure along (ξ_1, ξ_2) is *not* in general a uniform law over \mathbb{T}^2 . This is presented in detail in Section 2.1.

A motivation for considering dynamics (7) is that in the decoupled case, where

$$\begin{aligned} V(x_1, x_2, x_{3\dots n}) &= V(x_1) + V(x_2, x_{3\dots n}) \text{ or} \\ V(x_1, x_2, x_{3\dots n}) &= V(x_2) + V(x_1, x_{3\dots n}), \end{aligned} \quad (8)$$

then (7) is equivalent to (4). The key idea here is that, if the two reaction coordinates, ξ_1 and ξ_2 , are “not too strongly coupled”, then (7) should be as effective as (4), at a far reduced cost.

In Section 2, we propose a mathematical analysis of the long-time convergence of (7), which quantifies the underlying decoupling assumption. Section 3 is devoted to a discussion of some generalization of the idea of the present work, in particular to the case of m non-linear reaction coordinates with $m > 2$. Finally, in Section 4, we report two numerical illustrations on non-trivial test cases, which illuminate the interest and the limitation of the approach.

2 A convergence result

Let us introduce the Fokker-Planck equation associated to (7). Let us further refer $\psi(t, x)$ to as the density of the distribution of X_t . This function satisfies the partial differential equation:

$$\left\{ \begin{array}{l} \partial_t \psi = \operatorname{div}(\nabla V \psi + \beta^{-1} \psi) - \partial_{x_1}((A_t^1)'(x_1)\psi) - \partial_{x_2}((A_t^2)'(x_2)\psi), \\ (A_t^1)'(x_1) = \frac{\int \partial_{x_1} V(x) \psi(t, x) dx_2 dx_3 \dots n}{\int \psi(t, x) dx_2 dx_3 \dots n}, \\ (A_t^2)'(x_2) = \frac{\int \partial_{x_2} V(x) \psi(t, x) dx_1 dx_3 \dots n}{\int \psi(t, x) dx_1 dx_3 \dots n}. \end{array} \right. \quad (9)$$

where $(A_t^\alpha)'$ corresponds in what follows to the derivative of the one-dimensional function $x_\alpha \mapsto A_t^\alpha(x_\alpha)$.

2.1 Diffusive behavior

Let us introduce the marginal laws along x_1 and x_2 of ψ :

$$\psi^{x_1}(t, x_1) = \int \psi(t, x) dx_2 dx_3 \dots n \text{ and } \psi^{x_2}(t, x_2) = \int \psi(t, x) dx_1 dx_3 \dots n. \quad (10)$$

These marginal laws exhibit a simple diffusive behavior:

Proposition 1 *The probability distribution functions ψ^{x_1} and ψ^{x_2} satisfy the heat equation: for $\alpha \in \{1, 2\}$,*

$$\partial_t \psi^{x_\alpha} - \beta^{-1} \partial_{x_\alpha, x_\alpha} \psi^{x_\alpha} = 0 \text{ on } \mathbb{T}. \quad (11)$$

This property is easy to demonstrate by integrating the partial differential equation satisfied by ψ in (9) over the x_i , for $i \in \{1, \dots, n\} \setminus \{\alpha\}$.

As a simple consequence of (11), the marginal laws ψ^{x_1} and ψ^{x_2} converge to their equilibrium value $1_{\mathbb{T}}$ exponentially fast with rate

$$r = 4\pi^2,$$

for example in the following relative entropy sense (see Definition 1 below):

$$\int \psi^{x_\alpha}(t, \cdot) \ln(\psi^{x_\alpha}(t, \cdot)) \leq \int \psi^{x_\alpha}(0, \cdot) \ln(\psi^{x_\alpha}(0, \cdot)) \exp(-2\beta^{-1}rt). \quad (12)$$

2.2 Stationary state

If A_t^1 and A_t^2 reach a stationary state A_∞^1 and A_∞^2 , it is standard that the stationary probability distribution function in (9) is:

$$\psi_\infty(x) \propto \exp(-\beta(V(x) - A_\infty^1(x_1) - A_\infty^2(x_2))).$$

Thus, proving the existence of a stationary state is tantamount to proving the existence of a couple (A_∞^1, A_∞^2) solution to (note that the functions A_∞^α are defined up to an additive function):

$$\left\{ \begin{array}{l} (A_\infty^1)'(x_1) = \frac{\int \partial_{x_1} V(x) \exp(-\beta(V(x) - A_\infty^2(x_2))) dx_2 dx_3 \dots n}{\int \exp(-\beta(V(x) - A_\infty^2(x_2))) dx_2 dx_3 \dots n}, \\ (A_\infty^2)'(x_2) = \frac{\int \partial_{x_2} V(x) \exp(-\beta(V(x) - A_\infty^1(x_1))) dx_1 dx_3 \dots n}{\int \exp(-\beta(V(x) - A_\infty^1(x_1))) dx_1 dx_3 \dots n}. \end{array} \right. \quad (13)$$

Let us set

$$\rho^\alpha(x_\alpha) = \exp(-\beta A_\infty^\alpha(x_\alpha)).$$

Finding a solution to (13) is then equivalent to find a couple (ρ^1, ρ^2) solution to (note that the functions ρ^α are defined up to a multiplicative constant):

$$\begin{cases} \rho^1(x_1) = \int \frac{\exp(-\beta V(x))}{\rho^2(x_2)} dx_2 dx_{3\dots n}, \\ \rho^2(x_2) = \int \frac{\exp(-\beta V(x))}{\rho^1(x_1)} dx_1 dx_{3\dots n}. \end{cases} \quad (14)$$

Proposition 2 *Let us assume that V is a continuous function on \mathbb{T}^n . Then, there exists a solution to (14), and thus there exists a stationary state $(\psi_\infty, A_\infty^1, A_\infty^2)$ to (9).*

Proof : Let us build a sequence of continuous functions $\rho_n^1 : \mathbb{T} \rightarrow \mathbb{R}_+^*$ as $(\rho_0^1 = 1)$:

$$\rho_{n+1}^1(x_1) = Z_{n+1}^1 \int \frac{\exp(-\beta A(x_1, x_2))}{\int \frac{\exp(-\beta A(x_1, x_2))}{\rho_n^1(x_1)} dx_1} dx_2,$$

where Z_{n+1}^1 is chosen such that $\int 1/\rho_{n+1}^1(x_1) dx_1 = 1$ and A is the free energy (5) introduced above. It is clear that if $(\rho_n^1)_{n \geq 0}$ converges in $L^\infty(\mathbb{T})$ to ρ_∞^1 , then $\rho^1 = \rho_\infty^1$ and $\rho^2 = \int \frac{\exp(-\beta A(x_1, x_2))}{\rho_\infty^1(x_1)} dx_1$ is a solution to (14). We use the Arzelà–Ascoli theorem to show that $(\rho_n^1)_{n \geq 0}$ is a compact sequence in the space of real-valued continuous functions over \mathbb{T} , endowed with the L^∞ -norm, which concludes the existence proof.

It first ought to be noted that since V is continuous, there exists positive reals a, b such that $0 < a \leq \exp(-\beta A) \leq b$ on \mathbb{T}^2 . We, hence, have, for all $x_1 \in \mathbb{T}$,

$$\int \frac{\exp(-\beta A(x_1, x_2))}{\int \frac{\exp(-\beta A(x_1, x_2))}{\rho_n^1(x_1)} dx_1} dx_2 \geq \int \frac{\exp(-\beta A(x_1, x_2))}{b \int \frac{1}{\rho_n^1(x_1)} dx_1} dx_2 \geq \frac{a}{b}.$$

Likewise,

$$\int \frac{\exp(-\beta A(x_1, x_2))}{\int \frac{\exp(-\beta A(x_1, x_2))}{\rho_n^1(x_1)} dx_1} dx_2 \leq \frac{b}{a}.$$

>From this, one also obtains $\frac{a}{b} \leq Z_{n+1}^1 \leq \frac{b}{a}$ which implies: $\forall n \geq 0$,

$$\frac{a^2}{b^2} \leq \rho_n^1 \leq \frac{b^2}{a^2}.$$

The equicontinuity property remains to be checked to conclude the proof with the Arzelà–Ascoli theorem. This property is, however, straightforward to check by noting that

$$|\rho_n^1(x_1) - \rho_n^1(x'_1)| \leq \frac{b^2}{a^2} \int |\exp(-\beta A(x_1, x_2)) - \exp(-\beta A(x'_1, x_2))| dx_2.$$

◇

This altogether proves the existence of a stationary state. Its uniqueness is a consequence of the convergence result stated in the next section, which holds under an additional weak-coupling assumption (see (18) below).

A consequence of (14), which is also consistent with (11), is that the marginal probability density functions (see (10)) of ψ_∞ along x_1 and x_2 are uniform:

$$\psi_\infty^{x_1}(x_1) = \int \psi_\infty(x) dx_2 dx_{3\dots n} = 1 \text{ and } \psi_\infty^{x_2}(x_2) = \int \psi_\infty(x) dx_1 dx_{3\dots n} = 1.$$

Last, it is worth noting that by and large A_∞^1 and A_∞^2 are not the free energies associated to x_1 and x_2 and defined as — which should be compared with the definition of the bidimensional free energy (5):

$$\begin{aligned} A^1(x_1) &= -\beta^{-1} \ln \left(\int \exp(-\beta V(x_1, x_2, x_{3\dots n})) dx_2 dx_{3\dots n} \right), \\ A^2(x_2) &= -\beta^{-1} \ln \left(\int \exp(-\beta V(x_1, x_2, x_{3\dots n})) dx_1 dx_{3\dots n} \right). \end{aligned} \quad (15)$$

Actually, a special case for which $A_\infty^1 = A^1$ and $A_\infty^2 = A^2$ (up to additive constants) is the decoupled case, namely if the two-dimensional free energy A (defined by (5)) writes as a sum of a function of x_1 and a function of x_2 , which is equivalent, up to an additive constant, to:

$$A(x_1, x_2) = A^1(x_1) + A^2(x_2). \quad (16)$$

Under these premises, it is easy to check that $\rho^\alpha = \exp(-\beta A^\alpha)$ is the unique solution to (14), up to a multiplicative constant. It ought to be noted that (8) implies (16).

2.3 Convergence

Let us now consider a stationary state $(\psi_\infty, A_\infty^1, A_\infty^2)$ to (9). The aim of this section is to prove the convergence of (9) to this stationary state.

Let us first introduce the conditional probability density functions:

$$\psi_{\infty|x_1}(x_2, x_{3\dots n}) = \frac{\psi_\infty(x_1, x_2, x_{3\dots n})}{\psi_\infty^{x_1}(x_1)} = \psi_\infty(x_1, x_2, x_{3\dots n})$$

and

$$\psi_{\infty|x_2}(x_1, x_{3\dots n}) = \frac{\psi_\infty(x_1, x_2, x_{3\dots n})}{\psi_\infty^{x_2}(x_2)} = \psi_\infty(x_1, x_2, x_{3\dots n}).$$

In our particular case, this consists only in freezing one variable of ψ_∞ .

To achieve this objective, we will need tools related to logarithmic Sobolev inequalities. We recall that (see [3, 4, 57]):

Definition 1 *A probability measure ν is said to satisfy a logarithmic Sobolev inequality with constant $\rho > 0$ (in short: LSI(ρ)) if for all probability measures μ such that μ is absolutely continuous with respect to ν (denoted $\mu \ll \nu$ in the following),*

$$H(\mu|\nu) \leq \frac{1}{2\rho} I(\mu|\nu),$$

where

$$H(\mu|\nu) = \int \ln \left(\frac{d\mu}{d\nu} \right) d\mu$$

is the relative entropy of μ with respect to ν and

$$I(\mu|\nu) = \int \left| \nabla \ln \left(\frac{d\mu}{d\nu} \right) \right|^2 d\mu$$

is the so-called Fisher information of μ with respect to ν .

Since the measures $\psi_{\infty|x_1}(x_2, x_{3\dots n}) dx_2 dx_{3\dots n}$ and $\psi_{\infty|x_2}(x_1, x_{3\dots n}) dx_1 dx_{3\dots n}$ are defined on a compact space (\mathbb{T}^{n-1}) and since ψ_∞ is smooth, it follows from standard arguments — e.g. Holley-Stroock criterion, that they satisfy logarithmic Sobolev inequalities. Let us introduce the associated positive constants ρ_1 and ρ_2 :

$$\begin{aligned} &\psi_{\infty|x_1}(x_2, x_{3\dots n}) dx_2 dx_{3\dots n} \text{ (resp. } \psi_{\infty|x_2}(x_1, x_{3\dots n}) dx_1 dx_{3\dots n}) \text{ satisfies} \\ &\text{a LSI with constant } \rho_1 \text{ (resp. } \rho_2) \text{ for all } x_1 \in \mathbb{T} \text{ (resp. } x_2 \in \mathbb{T}). \end{aligned} \quad (17)$$

We also need to introduce the coupling constants

$$\kappa_1 = \|\nabla_{x_2, x_3, \dots, x_n}(\partial_{x_1} V)\|_{L^\infty(\mathbb{T}^n)} \text{ and } \kappa_2 = \|\nabla_{x_1, x_3, \dots, x_n}(\partial_{x_2} V)\|_{L^\infty(\mathbb{T}^n)}$$

which are well defined since V is assumed to be smooth over \mathbb{T}^n . It is worth noting that $\kappa_1 = 0$ or $\kappa_2 = 0$ is equivalent to (8), which implies the relation (16). This motivates the terminology of coupling constants.

For the convergence result to hold, we need the coupling constants to be sufficiently small compared to the logarithmic Sobolev constants ρ_1 and ρ_2 :

$$\rho_1 \rho_2 \geq \beta^2 \kappa_1 \kappa_2. \quad (18)$$

We are now in a position where we can state the main mathematical result of this contribution.

Theorem 1 *Let us assume (18). The probability density function $\psi(t, \cdot)$ then converges to ψ_∞ exponentially fast: for any $\varepsilon \in (0, \lambda)$, $\exists C > 0$, $\forall t \geq 0$*

$$\int_{\mathbb{T}^n} |\psi(t, x) - \psi_\infty(x)| dx \leq C \exp\left(-\beta^{-1} \min((\lambda - \varepsilon), r)t\right) \quad (19)$$

where $r = 4\pi^2$ and

$$\lambda = \frac{\rho_1 + \rho_2 - \sqrt{(\rho_1 - \rho_2)^2 + \frac{4\kappa_1 \kappa_2}{\rho_1 \rho_2}}}{4} \quad (20)$$

is a positive constant. Furthermore, for any positive time t_0 and $\varepsilon \in (0, \lambda)$, $\exists \bar{C} > 0$, $\forall t \geq t_0$,

$$\int_{\mathbb{T}} |(A_t^\alpha)' - (A_\infty^\alpha)'|^2 \leq \bar{C} \exp\left(-2\beta^{-1} \min((\lambda - \varepsilon), r)t\right), \quad (21)$$

where $\alpha \in \{1, 2\}$.

The interpretation of this theorem is that, if the coupling constants κ_1 and κ_2 are sufficiently small, the dynamics converges exponentially fast with a rate essentially limited by $\frac{\min(\rho_1, \rho_2)}{2}$ (namely λ when $\kappa_1 = 0$ or $\kappa_2 = 0$). This constant is expected to be larger than the logarithmic Sobolev constant of the original measure μ (which gives the rate of convergence of the original dynamics (2)) if ξ_1 and ξ_2 are well chosen — see related discussions in the work [38, 35].

Proof : The proof is an adaptation of the proof for the long-time convergence of the ABF process, which can be found in [38]. It can be assumed without loss of generality that $\beta = 1$ up to the following change of variable: $\tilde{t} = \beta^{-1}t$, $\tilde{\psi}(\tilde{t}, x) = \psi(t, x)$ and $\tilde{V}(x) = \beta V(x)$.

Let us first rewrite the partial differential equation satisfied by ψ as:

$$\partial_t \psi = \operatorname{div}\left(\psi \nabla \left(\frac{\psi}{\psi_\infty}\right)\right) + \partial_{x_1} \left(\left((A_\infty^1)'\right) - (A_t^1)'\right) \psi + \partial_{x_2} \left(\left((A_\infty^2)'\right) - (A_t^2)'\right) \psi.$$

Let us consider then the relative entropies

$$E(t) = H(\psi|\psi_\infty) = \int_{\mathbb{T}^n} \psi(t, \cdot) \ln(\psi(t, \cdot)/\psi_\infty)$$

and, for $\alpha \in \{1, 2\}$,

$$E_M^\alpha(t) = H(\psi^{x_\alpha}|\psi_\infty^{x_\alpha}) = \int_{\mathbb{T}} \psi^{x_\alpha}(t, \cdot) \ln(\psi^{x_\alpha}(t, \cdot)).$$

The aim of the present proof is to show that $E(t)$ converges to 0 exponentially fast. It is already clear from (11) that $E_M^\alpha(t)$ converges to zero exponentially fast (see (12)), so that it is enough to consider

$$E_m^\alpha(t) = E(t) - E_M^\alpha(t) = \int_{\mathbb{T}} H(\psi|_{x_\alpha}(t, \cdot)|\psi_\infty|_{x_\alpha}) \psi^{x_\alpha}(t, x_\alpha) dx_\alpha,$$

where

$$H(\psi_{|x_\alpha}(t, \cdot) | \psi_{\infty|x_\alpha}) = \int_{\mathbb{T}^{n-1}} \psi_{|x_\alpha}(t, \cdot) \ln(\psi_{|x_\alpha}(t, \cdot) / \psi_{\infty|x_\alpha})$$

is the relative entropy, with respect to $\psi_{\infty|x_\alpha}$, of the conditional probability density functions

$$\psi_{|x_1}(t, x_2, x_3 \dots n) = \frac{\psi(t, x_1, x_2, x_3 \dots n)}{\psi^{x_1}(t, x_1)} \text{ and } \psi_{|x_2}(t, x_1, x_3 \dots n) = \frac{\psi(t, x_1, x_2, x_3 \dots n)}{\psi^{x_2}(t, x_2)}.$$

Let us focus on the case $\alpha = 1$, albeit similar computations hold for $\alpha = 2$. Let us compute

$$\begin{aligned} \frac{dE_m^1}{dt} &= \frac{dE}{dt} - \frac{dE_M^1}{dt}, \\ &= - \int_{\mathbb{T}^n} \left| \nabla \ln \left(\frac{\psi}{\psi_\infty} \right) \right|^2 \psi + \sum_{\gamma=1}^2 \int_{\mathbb{T}^n} ((A_t^\gamma)' - (A_\infty^\gamma)') \partial_{x_\gamma} \ln \left(\frac{\psi}{\psi_\infty} \right) \psi \\ &\quad + \int_{\mathbb{T}} |\partial_{x_1} \ln(\psi^{x_1})|^2 \psi^{x_1}. \end{aligned} \quad (22)$$

It is rather easy to check the following identity:

$$(A_t^\alpha)' - (A_\infty^\alpha)' = \int_{\mathbb{T}^{n-1}} \partial_{x_\alpha} \ln \left(\frac{\psi}{\psi_\infty} \right) \frac{\psi}{\psi^{x_\alpha}} dx_{\bar{\alpha}} dx_{3 \dots n} - \partial_{x_\alpha} \ln(\psi^{x_\alpha}), \quad (23)$$

where $\bar{\alpha} = 1$ (resp. $\bar{\alpha} = 2$) when $\alpha = 2$ (resp. $\alpha = 1$). Using (23) in (22), we obtain

$$\begin{aligned} \frac{dE_m^1}{dt} &= - \int_{\mathbb{T}^n} \left| \partial_{x_2, x_3 \dots n} \ln \left(\frac{\psi}{\psi_\infty} \right) \right|^2 \psi \\ &\quad - \int_{\mathbb{T}^n} \left| \partial_{x_1} \ln \left(\frac{\psi}{\psi_\infty} \right) \right|^2 \psi + \int_{\mathbb{T}} \left(\int_{\mathbb{T}^{n-1}} \partial_{x_1} \ln \left(\frac{\psi}{\psi_\infty} \right) \psi dx_2 dx_3 \dots n \right)^2 \frac{1}{\psi^{x_1}} dx_1 \\ &\quad - \int_{\mathbb{T}^n} \partial_{x_1} \ln(\psi^{x_1}) \partial_{x_1} \ln \left(\frac{\psi}{\psi_\infty} \right) \psi + \int_{\mathbb{T}} |\partial_{x_1} \ln(\psi^{x_1})|^2 \psi^{x_1} \\ &\quad + \int_{\mathbb{T}^n} ((A_t^2)' - (A_\infty^2)') \partial_{x_2} \ln \left(\frac{\psi}{\psi_\infty} \right) \psi. \end{aligned}$$

By virtue of the Cauchy-Schwarz inequality, the term on the second line is non-positive. Using again (23), we, hence, have

$$\begin{aligned} \frac{dE_m^1}{dt} &\leq - \int_{\mathbb{T}^n} \left| \partial_{x_2, x_3 \dots n} \ln \left(\frac{\psi}{\psi_\infty} \right) \right|^2 \psi - \int_{\mathbb{T}} \partial_{x_1} \ln(\psi^{x_1}) \psi^{x_1} ((A_t^1)' - (A_\infty^1)') \\ &\quad + \int_{\mathbb{T}^n} ((A_t^2)' - (A_\infty^2)') \partial_{x_2} \ln \left(\frac{\psi}{\psi_\infty} \right) \psi. \end{aligned} \quad (24)$$

We now need an estimate for $|(A_t^1)' - (A_\infty^1)'|$. For any coupling measure $\pi \in \Pi(\psi_{|x_1}(t, \cdot), \psi_{\infty|x_1})$, it holds:

$$\begin{aligned} &|(A_t^1)'(x_1) - (A_\infty^1)'(x_1)| \\ &= \left| \int_{\mathbb{T}^{n-1} \times \mathbb{T}^{n-1}} (\partial_{x_1} V(x_1, x_2, x_3 \dots n) - \partial_{x_1} V(x_1, x'_2, x'_3 \dots n)) \pi(dx_2 dx_3 \dots n, dx'_2 dx'_3 \dots n) \right| \\ &\leq \|\nabla_{x_2, x_3 \dots n} (\partial_{x_1} V)\|_{L^\infty} \int_{\mathbb{R} \times \mathbb{R}} |(x_2, x_3 \dots n) - (x'_2, x'_3 \dots n)| \pi(dx_2 dx_3 \dots n, dx'_2 dx'_3 \dots n) \\ &\leq \kappa_1 \int_{\mathbb{R} \times \mathbb{R}} |(x_2, x_3 \dots n) - (x'_2, x'_3 \dots n)| \pi(dx_2 dx_3 \dots n, dx'_2 dx'_3 \dots n). \end{aligned}$$

Taking the infimum over all $\pi \in \Pi(\mu_{t,x}, \mu_{\infty,x})$, we obtain

$$|(A_t^1)'(x_1) - (A_\infty^1)'(x_1)| \leq \kappa_1 W(\psi_{|x_1}(t, \cdot), \psi_{\infty|x_1})$$

where W stands for the (L^1) Wasserstein distance. We will now resort to the fact that if ν is a probability measure satisfying a logarithmic Sobolev inequality with constant ρ , then we have the Talagrand inequality (see [6, 45]): For all probability measures μ such that $\mu \ll \nu$,

$$W(\mu, \nu) \leq \sqrt{\frac{2}{\rho} H(\mu|\nu)}.$$

Using (17) together with the Talagrand inequality, we, thus, obtain (the proof being evidently similar for $\alpha = 2$): for $\alpha \in \{1, 2\}$,

$$|(A_t^\alpha)'(x_\alpha) - (A_\infty^\alpha)'(x_\alpha)| \leq \kappa_\alpha \sqrt{\frac{2}{\rho_\alpha} H(\psi|_{x_\alpha}(t, \cdot) | \psi_\infty|_{x_\alpha})}. \quad (25)$$

Using this estimate in (24), the constants ρ_1 and ρ_2 introduced in (17), and Cauchy-Schwarz and Young inequalities, we get:

$$\begin{aligned} \frac{dE_m^1}{dt} &\leq -\frac{1}{2} \int_{\mathbb{T}^n} \left| \partial_{x_2, x_3, \dots, x_n} \ln \left(\frac{\psi}{\psi_\infty} \right) \right|^2 \psi + \sqrt{\int_{\mathbb{T}} |(A_t^1)' - (A_\infty^1)'|^2 \psi^{x_1}} \sqrt{\int_{\mathbb{T}} |\partial_{x_1} \ln(\psi^{x_1})|^2 \psi^{x_1}} \\ &\quad + \frac{1}{2} \int_{\mathbb{T}} |(A_t^2)' - (A_\infty^2)'|^2 \psi^{x_2} \\ &\leq -\rho_1 E_m^1 + \kappa_1 \sqrt{\frac{2}{\rho_1} E_m^1} \sqrt{I(\psi^{x_1} | \psi_\infty^{x_1})} + \frac{1}{2} \kappa_2^2 \frac{2}{\rho_2} E_m^2. \end{aligned}$$

Employing (11), it is standard to show that (see [38, Lemma 12] for example):

$$I(\psi^{x^1}(t, \cdot) | \psi_\infty^{x^1}) \leq I_0 \exp(-2rt)$$

where $I_0 = I(\psi^{x^1}(0, \cdot) | \psi_\infty^{x^1})$ and, we recall, $r = 4\pi^2$. We finally find for any positive η_1 :

$$\frac{dE_m^1}{dt} \leq -\rho_1(1 - \eta_1)E_m^1 + \frac{\kappa_2^2}{\rho_2} E_m^2 + \frac{\kappa_1^2}{2\rho_1^2 \eta_1} I_0 \exp(-2rt).$$

Utilizing a similar reasoning with $\alpha = 2$, the following system of inequalities is obtained, wherein η_1, η_2 are positive real numbers to be fixed:

$$\begin{cases} \frac{dE_m^1}{dt} \leq -\rho_1(1 - \eta_1)E_m^1 + \frac{\kappa_2^2}{\rho_2} E_m^2 + \frac{\kappa_1^2}{2\rho_1^2 \eta_1} I_0 \exp(-2rt), \\ \frac{dE_m^2}{dt} \leq -\rho_2(1 - \eta_2)E_m^2 + \frac{\kappa_1^2}{\rho_1} E_m^1 + \frac{\kappa_2^2}{2\rho_2^2 \eta_2} I_0 \exp(-2rt). \end{cases}$$

In the limit $\eta_1 = \eta_2 = 0$, we get the linear system:

$$\begin{cases} \frac{du^1}{dt} \leq -\rho_1 u^1 + \frac{\kappa_2^2}{\rho_2} u^2, \\ \frac{du^2}{dt} \leq -\rho_2 u^2 + \frac{\kappa_1^2}{\rho_1} u^1, \end{cases}$$

for which it can be shown quite simply that, under the assumption (18),

$$\forall t \geq 0, \|(u^1, u^2)(t)\| \leq \|(u^1, u^2)(0)\| \exp(-2\lambda t)$$

where λ is defined by (20). It is then easy to reach the result (19), employing the Csiszár-Kullback inequality:

$$\int |\psi - \psi_\infty| \leq \sqrt{2H(\psi | \psi_\infty)} \quad (26)$$

and the fact that $H(\psi | \psi_\infty) = E = E_M^\alpha + E_m^\alpha$. We refer the reader, for example, to the end of the proof of Theorem 1 in [36] for a similar reasoning.

Finally, the convergence results (21) on $(A_t^1)'$ and $(A_t^2)'$ are easily obtained from (25) and the fact that (using (11)) ψ^{x_1} and ψ^{x_2} are bounded from below by a positive constant for times larger than any arbitrary small positive time, see the beginning of Section 3.3.2 in [38] for more details. \diamond

3 Discussion and generalizations

3.1 The case of nonlinear reaction coordinates

We now would like to discuss generalizations of the approach introduced above, in the case where (ξ_1, ξ_2) are not simply (x_1, x_2) , which constitutes the vast majority of practical situations.

Let us denote $\xi_1 : \mathcal{D} \rightarrow \mathbb{T}$, and $\xi_2 : \mathcal{D} \rightarrow \mathbb{T}$, the chosen variables forming the multidimensional reaction coordinate. A natural generalization of (7) is the following:

$$\begin{cases} dX_t = -\nabla \left(V - \sum_{\alpha=1}^2 A_t^\alpha \circ \xi_\alpha \right) (X_t) dt + \sqrt{2\beta^{-1}} dB_t, \\ \text{for } \alpha = 1, 2, \frac{dA_t^\alpha}{dz_\alpha}(z_\alpha) = \mathbb{E}(f_t^\alpha(X_t) | \xi_\alpha(X_t) = z_\alpha), \end{cases} \quad (27)$$

where f_t^α stand for the so-called *local mean forces* associated to ξ_α and defined by:

$$f_t^1 = \left(\frac{\nabla(V - A_t^2 \circ \xi_2) \cdot \nabla \xi_1}{|\nabla \xi_1|^2} - \beta^{-1} \operatorname{div} \left(\frac{\nabla \xi_1}{|\nabla \xi_1|^2} \right) \right) \quad (28)$$

and

$$f_t^2 = \left(\frac{\nabla(V - A_t^1 \circ \xi_1) \cdot \nabla \xi_2}{|\nabla \xi_2|^2} - \beta^{-1} \operatorname{div} \left(\frac{\nabla \xi_2}{|\nabla \xi_2|^2} \right) \right). \quad (29)$$

It ought to be noted that (27) reduces to (7) in the specific case of $\xi_\alpha(x) = x_\alpha$.

If ψ denotes the probability density function of X_t , then the marginal probability density functions are:

$$\psi^{\xi_\alpha}(t, z_\alpha) = \int_{\Sigma^\alpha(z_\alpha)} \psi(t, x) \delta_{\xi_\alpha(x) - z_\alpha}(dx)$$

which boils down to (10) in the case of $\xi_\alpha(x) = x_\alpha$.

The conditional measure $\delta_{\xi_\alpha(x) - z_\alpha}(dx)$ obeys the following definition: For any test function $\varphi : \mathcal{D} \rightarrow \mathbb{R}$,

$$\int_{\mathcal{D}} \varphi(x) dx = \int_{\mathbb{T}} \int_{\Sigma^\alpha(z_\alpha)} \varphi(x) \delta_{\xi_\alpha(x) - z_\alpha}(dx) dz_\alpha,$$

where $\Sigma^\alpha(z_\alpha) = \{x \in \mathcal{D}, \xi_\alpha(x) = z_\alpha\}$. A corollary of the coarea formula is that:

$$\partial_{z_\alpha} \psi^{\xi_\alpha} = \int_{\Sigma^\alpha(z_\alpha)} \left(\frac{\nabla \psi \cdot \nabla \xi_\alpha}{|\nabla \xi_\alpha|^2} + \operatorname{div} \left(\frac{\nabla \xi_\alpha}{|\nabla \xi_\alpha|^2} \right) \psi \right) \delta_{\xi_\alpha(x) - z_\alpha}(dx). \quad (30)$$

For detailed proofs and references, the reader is referred to [39, Lemma 3.10].

One can check the following property, reminiscent of (11):

Proposition 3 *Let us assume that*

$$|\nabla \xi_1| = |\nabla \xi_2| = 1. \quad (31)$$

The probability distribution functions ψ^{ξ_1} and ψ^{ξ_2} satisfy the heat equation: for $\alpha \in \{1, 2\}$,

$$\partial_t \psi^{\xi_\alpha} - \beta^{-1} \partial_{z_\alpha, z_\alpha} \psi^{\xi_\alpha} = 0 \text{ on } \mathbb{T}. \quad (32)$$

Proof : Let us prove (32) for $\alpha = 1$, the proof being evidently similar for $\alpha = 2$. For

any test function $\varphi : \mathbb{T} \rightarrow \mathbb{R}$:

$$\begin{aligned}
\int_{\mathbb{T}} \partial_t \psi^{\xi_1} \varphi &= \int_{\mathcal{D}} \partial_t \psi \varphi \circ \xi_1 \\
&= \int_{\mathcal{D}} \operatorname{div} \left((\nabla(V - A_t^1 \circ \xi_1 - A_t^2 \circ \xi_2) \psi + \beta^{-1} \nabla \psi) \right) \varphi \circ \xi_1 \\
&= - \int_{\mathcal{D}} \left((\nabla(V - A_t^1 \circ \xi_1 - A_t^2 \circ \xi_2) \psi + \beta^{-1} \nabla \psi) \right) \cdot \nabla \xi_1 \varphi' \circ \xi_1 \\
&= - \int_{\mathcal{D}} \nabla(V - A_t^2 \circ \xi_2) \cdot \nabla \xi_1 \psi \varphi' \circ \xi_1 + \int_{\mathcal{D}} (A_t^1)' \circ \xi_1 \psi \varphi' \circ \xi_1 \\
&\quad - \beta^{-1} \int_{\mathcal{D}} \nabla \psi \cdot \nabla \xi_1 \varphi' \circ \xi_1 \\
&= - \int_{\mathcal{D}} \nabla(V - A_t^2 \circ \xi_2) \cdot \nabla \xi_1 \psi \varphi' \circ \xi_1 + \int_{\mathcal{D}} f_t^1 \psi \varphi' \circ \xi_1 \\
&\quad - \beta^{-1} \int_{\mathcal{D}} \nabla \psi \cdot \nabla \xi_1 \varphi' \circ \xi_1 \\
&= -\beta^{-1} \int_{\mathcal{D}} \Delta \xi_1 \psi \varphi' \circ \xi_1 - \beta^{-1} \int_{\mathcal{D}} \nabla \psi \cdot \nabla \xi_1 \varphi' \circ \xi_1 \\
&= -\beta^{-1} \int_{\mathbb{T}} \partial_{z_1} \psi^{\xi_1} \varphi',
\end{aligned}$$

where we used (30) for the last equality. This is, indeed, a weak formulation of (32). \diamond

Assumption (31) essentially amounts to assuming that ξ_α is the signed distance to $\Sigma^\alpha(0)$. It is straightforward to generalize the above result by changing the assumption (31) to: $|\nabla \xi_1|$ and $|\nabla \xi_2|$ are constant functions. It is also possible to generalize it to the case where $|\nabla \xi_1|$ (resp. $|\nabla \xi_2|$) depends on x only through $\xi_1(x)$ (resp. $\xi_2(x)$) with slight modifications of the definition of the functions f_t^α . Generalization of the convergence results of Theorem 1 to this setting is also possible, yet we will not pursue in this direction here.

3.2 The multi-dimensional setting

When more than two variables describing the multidimensional reaction coordinate are needed, the biasing procedure introduced above can be generalized as follows:

- (i) In the case of m collective variables ξ_1, \dots, ξ_m , a natural generalization would consist in biasing the dynamics by a potential $A_t^1 \circ \xi_1 + \dots + A_t^m \circ \xi_m$, using a straightforward extension of the dynamics (27). It is worth noting that the complexity is typically linear in m , whereas it is exponential in m for a standard ABF approach. For another biasing approach, in the context of multiple reaction coordinates, the reader is referred to [48].
- (ii) In the case of m collective variables, one might want to keep certain collective variables coupled, e.g. ξ_1 and ξ_2 . A natural way to build a biased dynamics in such a case consists in considering a biasing potential $A_t^{1,2} \circ (\xi_1, \xi_2) + A_t^3 \circ \xi_3 + \dots + A_t^m \circ \xi_m$, and using an adequate formula for updating $A_t^{1,2}$ based on the standard ABF approach (4) (see [39, Section 5.1.1] for example for adequate formulae for general (ξ_1, ξ_2)).

As mentioned above and roughly speaking, biasing the potential by the sum $A_t^1 \circ \xi_1 + \dots + A_t^m \circ \xi_m$ rather than by a m -dimensional adaptive potential $A_t \circ (\xi_1, \dots, \xi_m)$ — which would yield a perfect diffusion along the m -dimensional vector $(\xi^1, \dots, \xi^m)(X_t)$ — is tantamount to supposing some sort of decoupling on the collective variables ξ^1, \dots, ξ^m . More precisely, if the free energy associated to (ξ_1, \dots, ξ_m) writes as a sum of functions $A^1 \circ \xi_1 + \dots + A^m \circ \xi_m$, then the two algorithms (generalized-ABF and ABF) are equivalent. We, therefore, expect the method to be efficient if the collective

variables are loosely coupled, as would be the case for two dihedral angles distant from each other in a molecule. Conversely, should the two collective variables be more strongly coupled, it might be interesting to resolve this coupling in the adaptive potential, as discussed in item (ii) above.

3.3 Further generalizations

In practice, it may be difficult to implement the dynamics (27), in particular on account of the computations of the analytical expressions for f_t^α which may be cumbersome. A natural idea, which is, however, not supported by any mathematical reasoning, consists in simplifying the expressions for f_t^α , considering, for example:

$$f^1 = \left(\frac{\nabla V \cdot \nabla \xi_1}{|\nabla \xi_1|^2} - \beta^{-1} \operatorname{div} \left(\frac{\nabla \xi_1}{|\nabla \xi_1|^2} \right) \right), \quad (33)$$

or even

$$f^1 = \frac{\nabla V \cdot \nabla \xi_1}{|\nabla \xi_1|^2}, \quad (34)$$

and similar formulae for f^2 . A very practical approach can be stated as follows: *If* A_t^1 and A_t^2 happen to converge to some functions A_∞^1 and A_∞^2 , then it is always possible to fix this bias, and then to use unbiasing procedures akin to those described in Section 4.1 below — see (41), to obtain canonical averages.

4 Illustrations for free-energy calculations

In this section, we illustrate the interest and the limitation of the approach in two test cases, using the NAMD simulation package [47]. Propagation of motion is performed employing Langevin dynamics, in lieu of overdamped Langevin. Estimates of the biasing force rely upon trajectory, time averages rather than empirical averages over many replicas. Use is made of expression (33) to determine the local mean force. Overall, the method utilized here is similar to the biasing techniques (7)–(27) described above.

4.1 Recovering the free energy

To recover the free energy associated to some of the reaction coordinates chosen to bias the dynamics, one can simply use a grid of the values of the reaction coordinates, and classical formulas for the free energy or its derivative. This relies on the fact that from (7)–(27), if $((A_t^1)', (A_t^2)')$ reaches an equilibrium $((A_\infty^1)', (A_\infty^2)')$, then the law of X_t at equilibrium is proportional to $\exp(-\beta(V - A_\infty^1 \circ \xi_1 - A_\infty^2 \circ \xi_2))$.

Let us be more precise, considering (27). To get the free energy $A(z_1, z_2)$ associated to the bidimensional reaction coordinate (ξ_1, ξ_2) , one can use the formula (compare with (5) which is (35) in the simple case $(\xi_1, \xi_2) = (x_1, x_2)$):

$$A(z_1, z_2) = -\beta^{-1} \ln \int \exp(-\beta V(x)) \delta_{(\xi_1, \xi_2)(x) - (z_1, z_2)}(dx). \quad (35)$$

It is indeed easy to verify that, at equilibrium,

$$\lim_{\varepsilon \rightarrow 0} -\beta^{-1} \ln \mathbb{E}(\delta^\varepsilon((\xi_1, \xi_2)(X_t) - (z_1, z_2))) + A_\infty^1(z_1) + A_\infty^2(z_2) = A(z_1, z_2) \quad (36)$$

up to an additive constant. Here, δ^ε denotes an approximation of identity converging to a Dirac mass at 0 when ε goes to 0. In practice, piecewise constant approximation is obtained over a grid of values accessible to the reaction coordinates.

Another interesting formula to compute $A(z_1, z_2)$ derives from the formula:

$$\nabla A(z_1, z_2) = \mathbb{E}_\mu \left(F(X) | (\xi_1, \xi_2)(X) = (z_1, z_2) \right) \quad (37)$$

where the notation \mathbb{E}_μ means that X is distributed according to μ and F is a two-dimensional vector defined by: $\forall \alpha \in \{1, 2\}$,

$$F_\alpha = \sum_{\gamma=1}^2 G_{\alpha,\gamma}^{-1} \nabla \xi_\gamma \cdot \nabla V - \beta^{-1} \operatorname{div} \left(\sum_{\gamma=1}^2 G_{\alpha,\gamma}^{-1} \nabla \xi_\gamma \right), \quad (38)$$

where $G_{\alpha,\gamma}^{-1}$ denotes the (α, γ) -component of the inverse of the matrix with components: $\forall \alpha, \gamma \in \{1, 2\}$,

$$G_{\alpha,\gamma} = \nabla \xi_\alpha \cdot \nabla \xi_\gamma. \quad (39)$$

It is easy to check that if the time marginal law of X_t solution to (27) reaches an equilibrium, then

$$\mathbb{E} \left(F(X_t) | (\xi_1, \xi_2)(X_t) = (z_1, z_2) \right) = \nabla A(z_1, z_2). \quad (40)$$

At equilibrium, the law of X_t is, indeed, proportional to $\exp(-\beta(V - A_\infty^1 \circ \xi_1 - A_\infty^2 \circ \xi_2))$, which only differs from μ by a multiplicative function of (ξ_1, ξ_2) , which thus cancels out in the conditional average (40).

More generally, to estimate canonical averages, one may resort to the classical unbiasing procedure:

$$\int_{\mathcal{D}} \varphi d\mu = \frac{\int_{\mathcal{D}} \varphi \exp(-\beta(A_\infty^1 \circ \xi_1 + A_\infty^2 \circ \xi_2)) \psi_\infty}{\int_{\mathcal{D}} \exp(-\beta(A_\infty^1 \circ \xi_1 + A_\infty^2 \circ \xi_2)) \psi_\infty}, \quad (41)$$

where $\psi_\infty \propto \exp(-\beta(V - A_\infty^1 \circ \xi_1 - A_\infty^2 \circ \xi_2))$ stands for the density of the equilibrium time marginal law of X_t , once A_t^1 and A_t^2 have reached a stationary state. It is noteworthy that in practice, it is always possible to freeze A_t^1 and A_t^2 at a given fixed time t_0 and apply the unbiasing procedure above with the bias $A_{t_0}^1 \circ \xi_1 + A_{t_0}^2 \circ \xi_2$ instead of $A_\infty^1 \circ \xi_1 + A_\infty^2 \circ \xi_2$.

4.2 Conformational equilibrium of the alanine dipeptide

The first application of the method is a proof of concept making use of the prototypical terminally blocked amino acid N-acetyl-N'-methylalanylamine (NANMA), often referred to as alanine "dipeptide" [51]. The molecular system consisted of NANMA immersed in a bath of 447 water molecules. Conformational sampling was performed over a period of 10 ns with the numerical scheme described here, in which the ϕ and ψ torsional angles of the backbone were handled as independent order parameters covering each the $[-180; +180]$ range of the complete Ramachandran map [49]. In the present implementation of the method, the marginal biases, $A_\infty^1(\phi)$ and $A_\infty^2(\psi)$, are periodical — i.e. the average of their derivative is expected to zero out. As a basis of comparison, a two-dimensional ABF calculation was conducted over a period of 20 ns. For enhanced performances, the Ramachandran map was split into four individual quadrants, corresponding to fully independent simulations. Furthermore, a standard molecular-dynamics simulation of equal length was performed, from which the ϕ and ψ dihedral angles were extracted to measure the exhaustiveness of the conformational sampling.

The simulations were carried out using the NAMD simulation package [47] in the isobaric-isothermal ensemble. The pressure and the temperature were fixed at 1 bar and 300 K, respectively, employing the Langevin piston algorithm [20] and softly damped Langevin dynamics. The molecular system was replicated in the three directions of Cartesian space by means of periodic boundary conditions. The particle-mesh Ewald method [16] was employed to compute electrostatic interactions. The r -RESPA multiple time-step integrator [56] was used with a time step of 2 fs and 4 fs for short- and long-range forces, respectively. Covalent bonds involving a hydrogen atom were

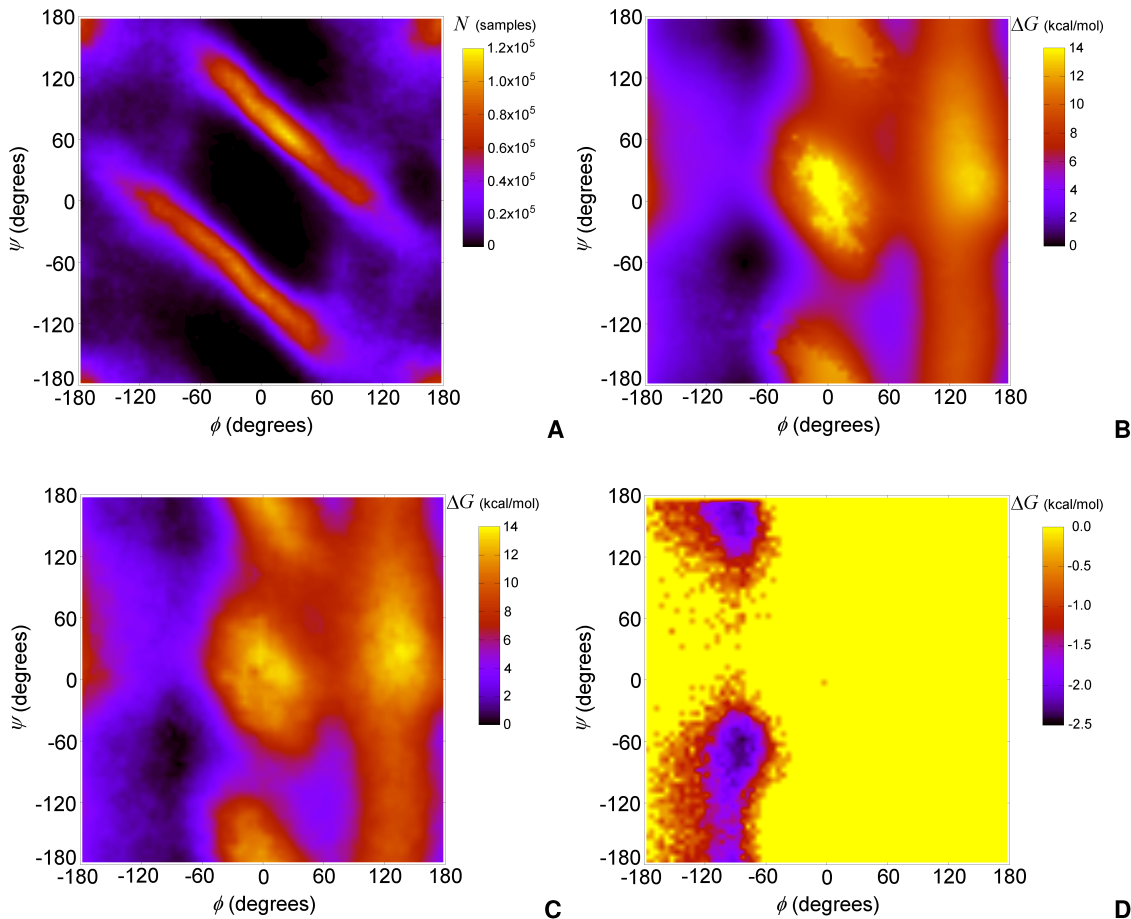


Figure 1: Conformational equilibrium of the alanine dipeptide (NANMA) in an aqueous solution. Distribution of the (ϕ, ψ) dihedral angles explored in the course of a 10-ns simulation, wherein the torsional angles of the backbone were handled as independent order parameter (A). Reconstruction of the conformational free-energy map, employing expression (36) (B). Conformational free-energy map obtained from a 20-ns, two-dimensional ABF calculation (C). For comparison purposes, a similar map was generated from a 20-ns unbiased MD simulation (D).

constrained to their equilibrium length. The short peptide and its environment were described by the all-atom CHARMM force field [41].

In the past thirty years, the conformational equilibrium of NANMA has been investigated at different levels of detail, utilizing a variety of numerical schemes and potential energy functions [24, 51, 9, 42, 50, 1, 55, 46, 44, 30, 13, 53, 7, 34, 2, 12, 40, 59, 31, 10, 43, 19]. Here, the investigation of NANMA is targeted at demonstrating the ability of the method to recover within reasonable sampling time the two-dimensional free-energy landscape that characterizes the conformational equilibrium of the peptide in an aqueous environment. As can be observed in Figure 1, within 10 ns, the essential features of the (ϕ, ψ) conformational space appear to have been explored. Plotting the number of samples accrued in the course of the simulation brings to light the anticipated coupling between the backbone torsional angles. Concomitant variation of the ϕ and ψ angles is mirrored in the two parallel diagonals, which appear to be oversampled. After convergence of the marginal biases, $A_{\infty}^1(\phi)$ and $A_{\infty}^2(\psi)$, the two-dimensional free-energy landscape was reconstructed employing Equation (36). Noteworthy, this map possesses the two expected pronounced minima corresponding to a right-handed α -helical conformation, often referred to as α_R , and to a β strand,

together with ancillary local minima of higher free energy, associated to the so-called α_D and α_L conformational states.

Integration over the basins delineating the α_R and the β conformations yields a free-energy difference of about 0.2 kcal/mol, in favor of the former state, congruent with previous computer simulations [55, 30, 13, 40, 59, 19]. Most importantly, the free-energy landscape inferred from the algorithm proposed herein is essentially identical to that obtained from a 20-ns ABF calculation in (ϕ, ψ) conformational space. A glimpse at Figure 1 is sufficient to conclude that not only the two maps appear to be almost interchangeable, but also, using the same bounds of integration over the α_R and the β basins, the free-energy differences agree quantitatively. It can, however, be contended that the present toy-example may be somewhat exaggeratedly simple to be representative of more challenging instances, wherein the variables along which the local mean force is computed are more strongly coupled. As has been discussed above, this scenario would constitute a limiting case for the validity of the approach developed in this contribution. Yet, as will be seen hereafter, estimators of the local mean force based on simulations handling unidimensional order parameters independently can still be used profitably to describe accurately rugged multidimensional free-energy landscapes wherein decoupling of the variables is not straightforward. Last, to illustrate the role of importance sampling methods, the (ϕ, ψ) -map regenerated from a 20-ns unbiased molecular-dynamics simulation. It is apparent from Figure 1 that only the lowest free-energy states, i.e. α_R and β , have been visited, though sampling is by and large too parsimonious to allow an acceptably precise free-energy difference to be determined.

4.3 Ion transport across a peptide nanotube

In the second application of the method proposed herein, translocation of an halide ion through a chemically-tailored peptide nanotube is considered. Such engineered synthetic channels arise from the self-assembly through an intermolecular hydrogen-bond network [8] of cyclic peptides of alternated D- and L-chirality [23, 25], in which all the side chains are pointing outwards. Depending upon its amino-acid sequence, the resulting anti-parallel β -sheet-like hollow tubular structure can further associate in the biological membrane with other channels to form nanopores, aggregate at the water-lipid interface prior to partitioning in the bilayer, disrupting in general the latter irreversibly, or simply span the membrane as an independent entity [22, 21]. Here, the peptide nanotube utilized consisted of eight stacked cyclic peptides containing alternated D-leucine and L-tryptophan residues and organized into *cyclo*[LW]₄ units [18]. At thermodynamic equilibrium, the cyclic peptides are 4.7 Å apart. The tubular structure was immersed in a fully hydrated, thermalized palmitoylcholine (POPC) bilayer formed by 48 lipid units in equilibrium with 1,572 water molecules. The molecular assembly was replicated in the three directions of Cartesian space. The initial dimensions of the simulation cell were $36 \times 41 \times 79$ Å³.

The free-energy landscape delineating permeation of a single chloride ion through the synthetic channel was determined along the longitudinal, ζ , and radial, ρ , directions of the latter [27]. The surrogate, two-dimensional reaction coordinate (ζ, ρ) was constructed as a subset of cylindrical polar coordinates, namely the distance separating the halide ion from the center of mass of the peptide nanotube projected onto its longitudinal axis, associated with the distance between the ion from this axis. Whereas the reaction pathway that connects the cytoplasm to the periplasm would span approximately 40 Å, the present investigation focuses on a 10-Å segment, starting from the center of mass of the open-ended tubular structure. This restrained pathway was discretized in 0.1-Å wide bins, in which force samples were accrued. The molecular-dynamics simulations were performed in the same conditions as described above for NANMA.

Chemically-engineered peptide nanotubes possess the ability of conducting ions [52]. Assuming an appropriate amino-acid sequence, individual tubular structures can insert in the lipid bilayer, where they act as transmembrane channels [32]. That such

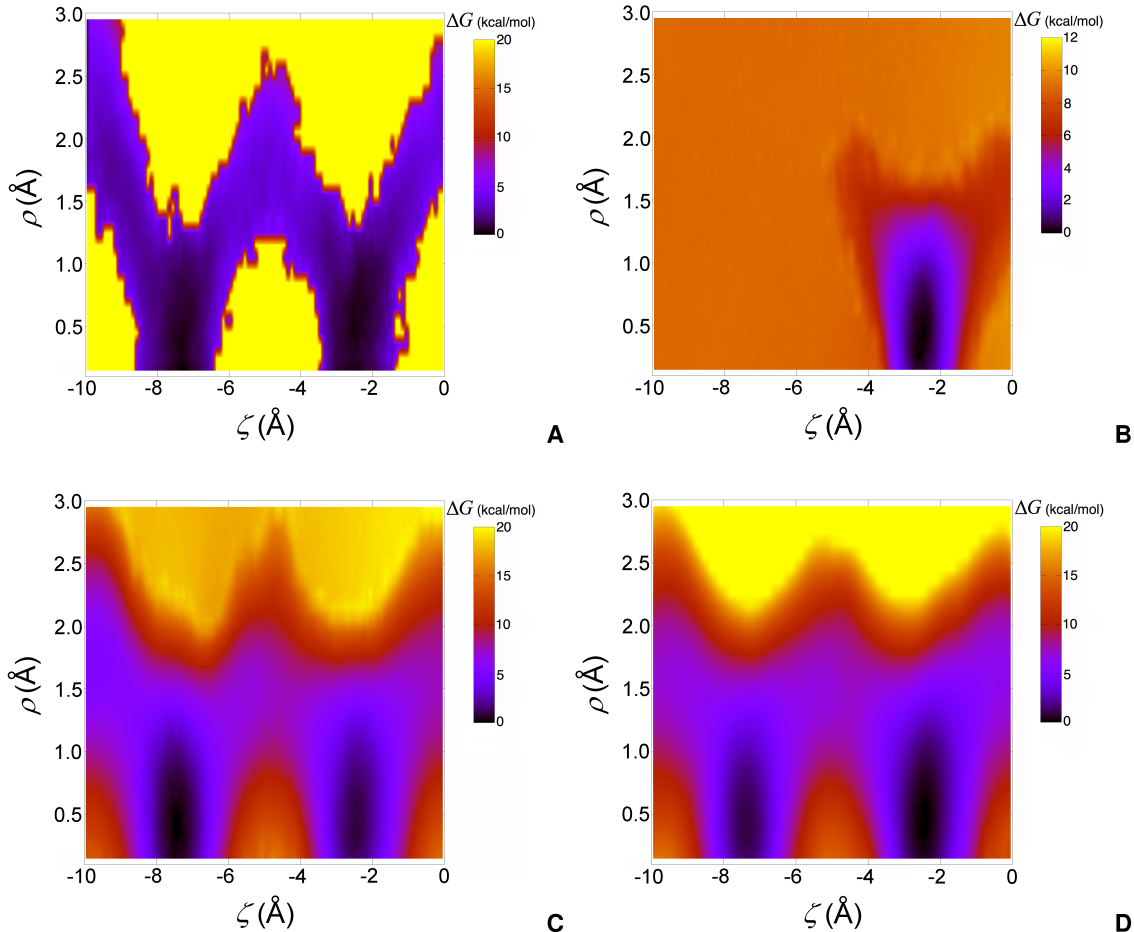


Figure 2: Permeation of a chloride ion through a peptide nanotube spanning a fully hydrated lipid bilayer. ζ denotes the longitudinal axis of the synthetic channel and ρ , the radial direction. Reconstruction employing expression (36) of the free-energy landscape of ion permeation after 1 ns of sampling in which ζ and ρ are treated as independent variables (A). Free-energy map obtained from a 1-ns two-dimensional ABF calculation (B). 10-ns ABF calculation, using as a starting point the two-dimensional gradients recovered from the 1-ns simulation in which ζ and ρ are handled independently and employing expression (37) (C). As a basis of comparison, (ζ, ρ) free-energy landscape inferred from a converged 30-ns two-dimensional ABF calculation (D). The lowest free-energy regions found at $\zeta = -2.4$ Å and $\zeta = -7.1$ Å correspond to an in-plane chelation of the halide ion, where the latter is located at the geometric center of the cyclic peptide.

channels can be permeated by a small ions has been investigated at the theoretical level, employing a variety of methods [5, 54, 28, 29]. It has been suggested recently that whereas diffusion of a sodium ion through a synthetic channel formed of eight *cyclo*[LW]₄ units and immersed in a fully hydrated POPC bilayer is essentially unhampered [18], the same cannot be said for a chloride ion shuttled across the cavity of an identical peptide nanotube [27]. This result can be rationalized to a large extent by the lesser hydration number of the cation — viz. approximately 4–6, compared to that of the halide ion — viz. approximately 6–8 [5], which must undergo considerable dehydration to enter the open-ended tubular structure. In the midst of the latter, however, the free-energy landscape characterizing ion permeation is roughly similar for both species, in-plane coordination being enthalpically favored because it allows the ion to be better hydrated [18].

As can be seen in Figure 2, this preference is reflected in the free-energy landscape obtained from the method proposed herein, handling ζ and ρ as independent variables. Within 1 ns of sampling, the entire reaction pathway is explored, following what appears to be a minimum-action path. It is noteworthy that the chloride ion does not diffuse along a rectilinear path, collinear to the longitudinal axis of the synthetic channel, e.g. at $\zeta = 0 \text{ \AA}$, but rather avoids the large free-energy barrier of mid-plane coordination by grazing the wall of the tubular structure to interact with the amino groups of the *cyclo*[LW]₄ units. Repeated simulations, using different initial momenta, yield comparable landscapes, yet wherein the higher free-energy regions are essentially never visited. Interestingly enough, the free-energy minima found at about -2.4 and -7.1 \AA have virtually the same depth. It is remarkable that a limited simulation length of 1 ns would provide a consistent picture of the path followed by the chloride ion over the 10-\AA stretch of the peptide nanotube, when repeated two-dimensional ABF calculations of equal length only sample a small fraction of the (ζ, ρ) configurational space, as shown in Figure 2.

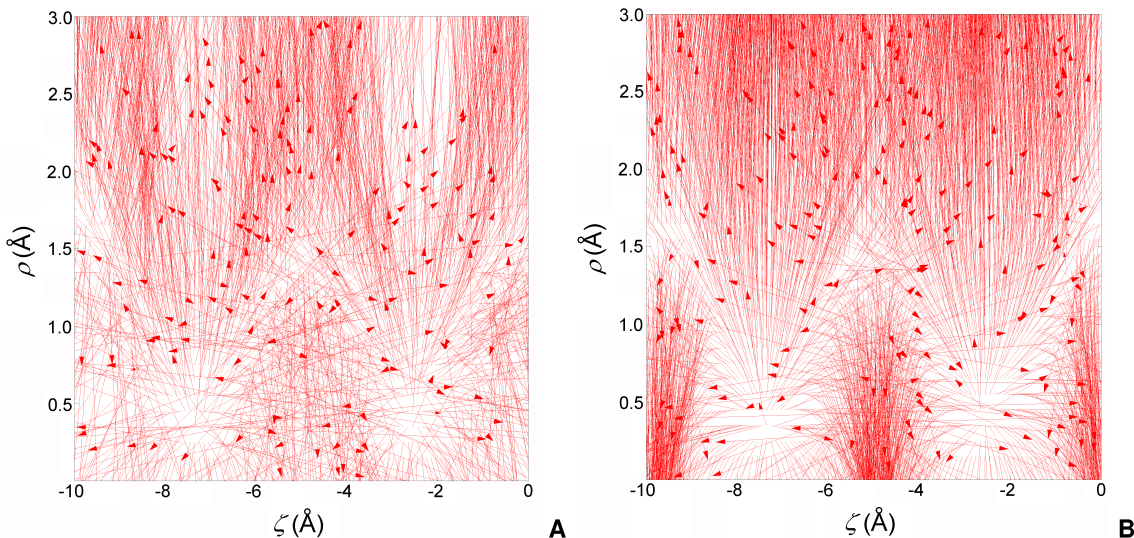


Figure 3: Permeation of a chloride ion through a peptide nanotube spanning a fully hydrated lipid bilayer. ζ denotes the longitudinal axis of the synthetic channel and ρ , the radial direction. Gradient of the free energy inferred from a 1-ns simulation wherein ζ and ρ are handled independently, employing expression (37) (A). For comparison purposes, two-dimensional gradient of the free energy obtained from a 30-ns ABF calculation in (ζ, ρ) configurational space (B).

Unfortunately, while the ABF calculation progressively explores the free-energy landscape of ion permeation, reaching convergence within 30 ns, a simulation of equal length based on the numerical scheme introduced here only marginally improves the picture drawn from the aforementioned short 1-ns run. This glaring shortcoming of the method can be ascribed in large measure to antagonist effects of the biases in the ζ and in the ρ directions, deteriorating mutually any progress made by the two variables. It does not mean, however, that the valuable, yet incomplete description of the reaction pathway cannot be utilized profitably to recover the correct free-energy landscape, possibly faster than a classical ABF calculation would.

As has been discussed previously, Equation (37) allows the gradient of the free energy to be estimated on the basis of independent measures of the force acting along the two order parameters, ζ and ρ . In Figure 3, the reference two-dimensional gradient of the free energy inferred from a 30-ns ABF calculation is compared to an approximation thereof obtained after 1 ns of sampling. Although the two vector fields show significant discrepancies, they also retain common characteristic features, in particular in the region of lower free energy, visited appropriately by the algorithm described

herein. In turn, the approximate gradient can be employed as a starting point for a separate ABF calculation in (ζ, ρ) configurational space, with the hope that the initial guess of a minimum-action pathway might boost exploration of the complete free-energy landscape. As highlighted in Figure 2, this appears to be, indeed, true — after 10 ns, the map inferred from the separate two-dimensional ABF run possesses a topology essentially identical to that of the reference, 30-ns simulation. However not interchangeable, the two free-energy landscapes agree quantitatively in the low free-energy regions — i.e $0 \leq \rho \leq 2 \text{ \AA}$, albeit only qualitatively so in the higher free-energy regions corresponding to the wall of the open-ended tubular structure.

Acknowledgments.

The authors gratefully acknowledge Jérôme Hénin for stimulating discussions. They are indebted to the Grand Équipement National de Calcul Intensif and the Centre Informatique National de l’Enseignement Supérieur for provision of computer time. This work is funded by the Agence Nationale de la Recherche (MEGAS project, grant ANR-09-BLAN-0216-01) and the Institut National de la Recherche en Informatique et en Automatique (ARC Hybrid project).

References

- [1] A. Anderson and J. Hermans. Microfolding: Conformational probability map for the alanine dipeptide in water from molecular dynamics simulations. *Proteins: Structure, Function and Genetics*, 3:262–265, 1988.
- [2] I. Andricioaei, A. R. Dinner, and M. Karplus. Self-guided enhanced sampling methods for thermodynamic averages. *J. Chem. Phys.*, 118:1074–1084, 2003.
- [3] C. Ané, S. Blachère, D. Chafaï, P. Fougères, I. Gentil, F. Malrieu, C. Roberto, and G. Scheffer. *Sur les inégalités de Sobolev logarithmiques*. Société Mathématique de France, 2000. In French.
- [4] A. Arnold, P. Markowich, G. Toscani, and A. Unterreiter. On convex Sobolev inequalities and the rate of convergence to equilibrium for Fokker-Planck type equations. *Comm. Part. Diff. Eq.*, 26:43–100, 2001.
- [5] D. Asthagiri and D. Bashford. Continuum and atomistic modeling of ion partitioning into a peptide nanotube. *Biophys. J.*, 82:1176–1189, 2002.
- [6] S. Bobkov and F. Götze. Exponential integrability and transportation cost related to logarithmic Sobolev inequalities. *J. Funct. Anal.*, 163(1):1–28, 1999.
- [7] P. G. Bolhuis, C. Dellago, and D. Chandler. Reaction coordinates of biomolecular isomerization. *Proc. Natl. Acad. Sci. U. S. A.*, 97:5877–5882, 2000.
- [8] D. T. Bong, T. D. Clark, J. R. Granja, and M. R. Ghadiri. Self-assembling organic nanotubes. *Angew. Chem. Int. Ed. Engl.*, 40:988–1011, 2001.
- [9] J. Brady and M. Karplus. Configuration entropy of the alanine dipeptide in vacuum and in solution: A molecular dynamics study. *J. Am. Chem. Soc.*, 107:6103–6105, 1985.
- [10] D. Branduardi, F. L. Gervasio, and M. Parrinello. From a to b in free energy space. *J. Chem. Phys.*, 126:054103, 2007.
- [11] G. Bussi, A. Laio, and M. Parrinello. Equilibrium free energies from nonequilibrium metadynamics. *Phys. Rev. Lett.*, 96:090601, 2006.
- [12] D.S. Chekmarev, T. Ishida, and R. M. Levy. Long-time conformational transitions of alanine dipeptide in aqueous solution: Continuous and discrete-state kinetic models. *J. Phys. Chem. B*, 108:19487–19495, 2004.
- [13] C. Chipot and A. Pohorille. Conformational equilibria of terminally blocked single amino acids at the water-hexane interface. a molecular dynamics study. *J. Phys. Chem. B*, 102:281–290, 1998.

- [14] C. Chipot and A. Pohorille, editors. *Free Energy Calculations*, volume 86 of *Springer Series in Chemical Physics*. Springer, 2007.
- [15] N. Chopin, T. Lelièvre, and G. Stoltz. Free energy methods for efficient exploration of mixture posterior densities, 2010. Available at <http://fr.arxiv.org/abs/1003.0428>.
- [16] T. A. Darden, D. M. York, and L. G. Pedersen. Particle mesh ewald: An *nlogn* method for ewald sums in large systems. *J. Chem. Phys.*, 98:10089–10092, 1993.
- [17] E. Darve and A. Porohille. Calculating free energy using average forces. *J. Chem. Phys.*, 115:9169–9183, 2001.
- [18] F. Dehez, M. Tarek, and C. Chipot. Energetics of ion transport in a peptide nanotube. *J. Phys. Chem. B*, 111:10633–10635, 2007.
- [19] M. Feig. Is alanine dipeptide a good model for representing the torsional preferences of protein backbones? *J. Chem. Theor. Comput.*, 4:1555–1564, 2008.
- [20] S. E. Feller, Y. H. Zhang, R. W. Pastor, and B. R Brooks. Constant pressure molecular dynamics simulations — the langevin piston method. *J. Chem. Phys.*, 103:4613–4621, 1995.
- [21] S. Fernandez-Lopez, H. S. Kim, E. C. Choi, M. Delgado, J. R. Granja, A. Khasanov, K. Kraehenbuehl, G. Long, D. A. Weinberger, K. M. Wilcoxon, and M. R. Ghadiri. Antibacterial agents based on the cyclic D, L- α -peptide architecture. *Nature*, 412:452–455, 2001.
- [22] M. R. Ghadiri, J. R. Granja, and L. K. Buehler. Artificial transmembrane ion channels from self-assembling peptide nanotubes. *Nature*, 369:301–304, 1994.
- [23] M. R. Ghadiri, J. R. Granja, R. A. Milligan, D. E. McRee, and N. Khazanovich. Self-assembling organic nanotubes based on a cyclic peptide architecture. *Nature*, 366:324–327, 1993.
- [24] A. T. Hagler and B. Honig. On the formation of protein tertiary structure on a computer. *Proc. Natl. Acad. Sci. USA*, 75:554–558, 1978.
- [25] J. D. Hartgerink, J. R. Granja, R. A. Milligan, and M. R. Ghadiri. Self-assembling peptide nanotubes. *J. Am. Chem. Soc.*, 118:43–50, 1996.
- [26] J. Hénin and C. Chipot. Overcoming free energy barriers using unconstrained molecular dynamics simulations. *J. Chem. Phys.*, 121:2904–2914, 2004.
- [27] J. Hénin, G. Forin, C. Chipot, and M. L. Klein. Exploring multidimensional free energy landscapes using time-dependent biases on collective variables. *J. Chem. Theor. Comput.*, 6:35–47, 2010.
- [28] H. Hwang, G. C. Schatz, and M. A. Ratner. Ion current calculations based on three dimensional Poisson-Nernst-Planck theory for a cyclic peptide nanotube. *J. Phys. Chem. B*, 110:6999–7008, 2006.
- [29] H. Hwang, G. C. Schatz, and M. A. Ratner. Steered molecular dynamics studies of the potential of mean force of a Na^+ or K^+ ion in a cyclic peptide nanotube. *J. Phys. Chem. B*, 110:26448–26460, 2006.
- [30] J. A. McCammon J. L. Smart, T. J. Marrone. Conformational sampling with poisson-boltzmann forces and a stochastic dynamics/monte carlo method: Application to alanine dipeptides. *J. Comput. Chem.*, 18:1750–1759, 1997.
- [31] H. Jang and T. B Woolf. Multiple pathways in conformational transitions of the alanine dipeptide: an application of dynamic importance sampling. *J. Comput. Chem.*, 27:1136–1141, 2006.
- [32] H. S. Kim, J. D. Hartgerink, and M. R. Ghadiri. Oriented self-assembly of cyclic peptide nanotubes in lipid membranes. *J. Am. Chem. Soc.*, 120:4417–4424, 1998.
- [33] A. Laio and M. Parinello. Escaping free-energy minima. *Proc. Natl. Acad. Sci. U.S.A.*, 99:12562–12566, 2002.

- [34] A. Laio and M. Parrinello. Escaping free energy minima. *Proc. Natl. Acad. Sci. USA*, 99:12562–12565, 2002.
- [35] T. Lelièvre. A general two-scale criteria for logarithmic Sobolev inequalities. *Journal of Functional Analysis*, 256(7):2211–2221, 2009.
- [36] T. Lelièvre and K. Minoukadeh. Long-time convergence of an adaptive biasing force method: the bi-channel case, 2010. <http://arxiv.org/abs/1005.0206>.
- [37] T. Lelièvre, M. Rousset, and G. Stoltz. Computation of free energy profiles with adaptive parallel dynamics. *J. Chem. Phys.*, 126:134111, 2007.
- [38] T. Lelièvre, M. Rousset, and G. Stoltz. Long-time convergence of an adaptive biasing force method. *Nonlinearity*, 21:1155–1181, 2008.
- [39] T. Lelièvre, M. Rousset, and G. Stoltz. *Free energy computations: A mathematical perspective*. Imperial College Press, 2010.
- [40] Alexander D MacKerell, Michael Feig, and Charles L Brooks. Improved treatment of the protein backbone in empirical force fields. *J. Am. Chem. Soc.*, 126(3):698–9, 2004.
- [41] A. D. MacKerell Jr., D. Bashford, M. Bellott, R. L. Dunbrack Jr., J. D. Evanseck, M. J. Field, S. Fischer, J. Gao, H. Guo, S. Ha, D. Joseph-McCarthy, L. Kuchnir, K. Kuczera, F. T. K. Lau, C. Mattos, S. Michnick, T. Ngo, D. T. Nguyen, B. Prodhom, W. E. Reiher III, B. Roux, M. Schlenkrich, J. C. Smith, R. Stote, J. Straub, M. Watanabe, J. Wiórkiewicz-Kuczera, D. Yin, and M. Karplus. All-atom empirical potential for molecular modeling and dynamics studies of proteins. *J. Phys. Chem. B*, 102:3586–3616, 1998.
- [42] M. Mezei, P. K. Mehrotra, and D. L. Beveridge. Monte-carlo determination of the free energy and internal energy of hydration for the ala dipeptide at 25^circc. *J. Am. Chem. Soc.*, 107:2239–2245, 1985.
- [43] C. Neale, T. Rodinger, and R. Pomès. Equilibrium exchange enhances the convergence rate of umbrella sampling. *Chem. Phys. Lett.*, 460:375–381, 2008.
- [44] E. Neria, S. Fischer, and M. Karplus. Simulation of activation free energies in molecular systems. *J. Chem. Phys.*, 105:1902, 1996.
- [45] F. Otto and C. Villani. Generalization of an inequality by Talagrand and links with the logarithmic Sobolev inequality. *J. Funct. Anal.*, 173(2):361–400, 2000.
- [46] M. Pellegrini, N. Grønbech-Jensen, and S. Doniach. Potentials of mean force for biomolecular simulations: Theory and test on alanine dipeptides. *J. Chem. Phys.*, 104:8639–8648, 1996.
- [47] J. C. Phillips, R. Braun, W. Wang, J. Gumbart, E. Tajkhorshid, E. Villa, C. Chipot, L. Skeel, R. D. Kalé, and K. Schulten. Scalable molecular dynamics with NAMD. *J. Comput. Chem.*, 26:1781–1802, 2005.
- [48] S. Piana and A. Laio. A bias-exchange approach to protein folding. *J. Phys. Chem. B*, 111(17):4553–4559, 2007.
- [49] G.N. Ramachandran, C. Ramakrishnan, and V. Sasisekharan. Stereochemistry of polypeptide chain configurations. *J. Mol. Biol.*, 7:95–99, 1963.
- [50] G. Ravishanker, M. Mezei, and D. L. Beveridge. Conformational stability and flexibility of the ala dipeptide in free space and in water: Monte carlo computer simulation studies. *J. Comput. Chem.*, 7:345–348, 1986.
- [51] P. J. Rossky and M. Karplus. Solvation. a molecular dynamics study of a dipeptide in water. *J. Am. Chem. Soc.*, 101:1913–1937, 1979.
- [52] J. Sánchez-Quesada, M. P. Isler, and M. R. Ghadiri. Modulating ion channel properties of transmembrane peptide nanotubes through heteromeric supramolecular assemblies. *J. Am. Chem. Soc.*, 124:10004–10005, 2002.
- [53] P. E. Smith. The alanine dipeptide free energy surface in solution. *J. Chem. Phys.*, 111:5568–5579, 1999.

- [54] M. Tarek, B. Maigret, and C. Chipot. Molecular dynamics investigation of an oriented cyclic peptide nanotube in DMPC bilayers. *Biophys. J.*, 85:2287–2298, 2003.
- [55] D. J. Tobias and C. L. Brooks. Conformational equilibrium in the alanine dipeptide in the gas phase and aqueous solution: A comparison of theoretical results. *J. Phys. Chem.*, 96:3864–3870, 1992.
- [56] M. E. Tuckerman, B. J. Berne, and G. J. Martyna. Reversible multiple time scale molecular dynamics. *J. Phys. Chem. B*, 97:1990–2001, 1992.
- [57] C. Villani. *Topics in optimal transportation*, volume 58 of *Graduate Studies in Mathematics*. American Mathematical Society, 2003.
- [58] F. Wang and D.P. Landau. Determining the density of states for classical statistical models: A random walk algorithm to produce a flat histogram. *Phys. Rev. E*, 64:056101, 2001.
- [59] Y. Duan Z. Wang. Solvation effects on alanine dipeptide: A mp2/cc-pvtz//mp2/6-31g** study of (ϕ, ψ) energy maps and conformers in the gas phase, ether, and water. *J. Comput. Chem.*, 25:1699–1716, 2004.